Energy Harvester Synthesis Via Coupled Linear-Bistable System With Multistable Dynamics

Z. Wu[1]
Department of Mechanical Engineering,
University of Michigan,
Ann Arbor, MI 48109-2125

R. L. Harne
Department of Mechanical Engineering,
University of Michigan,
Ann Arbor, MI 48109-2125

K. W. Wang
Department of Mechanical Engineering,
University of Michigan,
Ann Arbor, MI 48109-2125

In this research we study the dynamics of a coupled linear oscillator-bistable energy harvester system. The method of harmonic balance and perturbation analysis are used to predict the existence and stability of the bistable device interwell vibration. The influences of important parameters on tailoring the coupled system response are investigated to determine strategies for improved energy harvesting performance. We demonstrate analytically that for excitation frequencies in a bandwidth less than the natural frequency of the uncoupled linear oscillator having net mass that is the combination of the bistable and linear bodies, the bistable harvester dynamics may be substantially intensified as compared to a single (individual) bistable harvester. In addition, the linear-bistable coupled system may introduce a stable out-of-phase dynamic around the natural frequency of the uncoupled linear oscillator, enhancing the performance of the harvester by providing a second interwell response not possible when using a single bistable harvester. Key analytical findings are confirmed through numerical simulations and experiments, validating the predicted trends and demonstrating the advantages of the coupled system for energy harvesting. [DOI: 10.1115/1.4026555]

Keywords: vibration energy harvesting, bistable snap through, coupled linear–nonlinear dynamics

1 Introduction

1.1 Background. In recent years the proliferation of portable electronics and wireless sensors has grown rapidly due to advances in microelectronic technology. Many of the devices are powered by batteries which have a finite lifespan. This can inhibit the use of such electronics in remote or inaccessible environments because replacing batteries may be costly if not impossible. Hence, the concept of exploiting self-powered or energy harvesting devices as an alternative to batteries has attracted much attention from researchers [1].

Energy harvesting commonly refers to the process of converting a renewable environmental energy resource into electrical power. El-Hami et al. [2], Roundy et al. [3], and Mitcheson et al. [4] proposed early solutions for the conversion of vibrating potential to electric energy. Much of the initial research focused on linear resonant vibration harvesters which are most effective at a specific frequency. If the excitation frequency shifts, the performance of the harvester will drop dramatically. This limits the utility of such designs due to the broad bandwidth of energy in the environmental vibration spectrum [3]. Therefore, considerable study has focused on broadening the frequency range for vibrational energy harvesters [5,6]. Inspired by the field of vibration control [7,8], research in vibrational energy harvesting has also explored linear multidegree-of-freedom (MDOF) dynamic systems to enhance the operational bandwidth and increase the number of attainable dynamic features. Configurations such as multimode harvesters [9,10], "dynamic magnifier" [11–13], and dual-mass harvesters [14,15] have exemplified the benefits of a systems-level design approach to yield harvesting performance extending beyond that achievable with single degree-of-freedom (SDOF) elements.

Bistable devices have been explored for energy harvesting performance and bandwidth enhancement due to advantageous interwell or high-energy dynamics: a dynamic response during which the inertial mass oscillates between its two equilibria [16–22]. Additionally, they are more robust to manufacturing defects and may be more useful in realistic vibration environments than linear or monostable nonlinear harvester designs [17,23]. Owing to these advantages, bistable harvesters have recently experienced a drastic increase in attention [24].

Taking a cue from related energy harvesting literature that studied the advantage of auxiliary add-on DOF for harvester enhancement [25], Harne et al. [26] investigated the dynamics of an excited bistable harvester with an appendage linear oscillator. It was demonstrated that the benefit of this design methodology was an intensifying of the snap through, interwell dynamics. Given this promising result and in light of the advantages obtained when adopting a system-level perspective for linear MDOF harvesters [9–13], we consider a new approach to the bistable energy harvester system in expectation of attaining both amplified high-energy vibration and new dynamics that are not achievable in previous studied configurations.

1.2 Problem Statement and Research Objectives. Our present holistic approach to the bistable harvester system follows that of linear dynamic magnifier energy harvesting investigations [11–13]: we utilize a linear resonator between the excitation and the bistable harvester, depicted in Fig. 1. Tuned appropriately, the coupled system should be capable of achieving high-orbit or high-energy dynamics when otherwise the individual bistable oscillator attains only low-orbit or low-energy response. As compared to the different add-on configuration and framework discussed in [26], we seek to uncover new dynamics that have not been observed or studied previously, in a manner similar to the multimode response of linear dynamic magnifier harvesters. While the proposed idea is intuitively reasonable, a thorough study is needed to examine the feasibility of the concept, provide guidelines for system synthesis, and develop insights to enhance the energy harvesting

[1]Corresponding author: wuzhen@umich.edu
Manuscript received February 21, 2013; final manuscript received January 20, 2014; accepted manuscript posted January 27, 2014; published online February 10, 2014. Assoc. Editor: Alexander F. Vakakis.

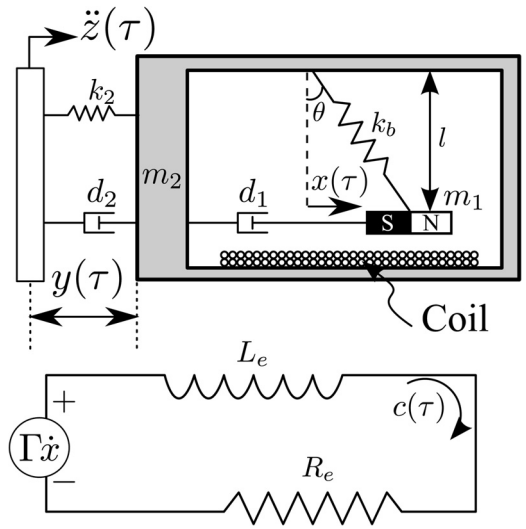

Fig. 1 Base-excited linear oscillator with attached bistable energy harvester having transduction mechanism and corresponding harvesting circuit

performance. The present investigation seeks to achieve these technical objectives, employing harmonic balance (HB) and Jacobian analysis together with experimental and numerical studies.

2 Mathematical Formulation of the Coupled Linear Oscillator-Bistable Energy Harvester System

2.1 Governing Equations. As depicted in Fig. 1, consider an electromagnetic bistable oscillator of moving magnetic mass m_1 which is coupled to a linear oscillator of mass m_2. It is assumed that motion of the bistable harvester does not encounter stroke limitations by way of its integration to or within the linear oscillator. The linear element is harmonically excited through base acceleration $\ddot{z}(\tau) = -Z_0\cos(\Omega\tau)$. The axial restoring force is given by

$$F(x) = k_b\left(\sqrt{x^2+l^2} - l_o\right)\sin(\theta) \tag{1}$$

where k_b, l_0 are the stiffness and free length of the spring; l is the vertical distance between linear frame and bistable mass; and θ is the inclination of the spring measured from the unstable equilibrium position of the bistable harvester ($x = 0$), where $\sin(\theta) = x/\sqrt{x^2+l^2}$, indicated in Fig. 1. Assuming $x/l \ll 1$, by a binomial series expansion, the restoring force can be simplified to

$$F = k_b\left(1 - \frac{l_o}{l}\right)x + \frac{k_b l_o}{2l^3}x^3 + O\left(x^5\right) \tag{2}$$

The governing equations for the system are then expressed as

$$m_1(\ddot{x}+\ddot{y}+\ddot{z}) + d_1\dot{x} - k_1x + k_3x^3 + \Gamma c = 0 \tag{3}$$

$$m_2(\ddot{z}+\ddot{y}) + d_2\dot{y} + k_2y - d_1\dot{x} + k_1x - k_3x^3 - \Gamma c = 0 \tag{4}$$

$$L_e\dot{c} + R_e c = \Gamma\dot{x} \tag{5}$$

where x is the relative displacement between the linear oscillator mass and bistable inertial mass; y is the relative displacement between the linear oscillator and base; c is the current flow through resistance R_e which represents the load of a generalized energy harvesting circuitry; L_e is the inductance of electromagnetic generator; Γ is an electromagnetic coupling constant; d_1 and d_2 are mechanical damping; $k_1 = k_b((l_o/l) - 1)$ and $k_3 = (k_b l_o/2l^3)$ are linear and nonlinear stiffness of the bistable harvester, respectively; and the overdot is differentiation with respect to time τ.

After substitution of Eqs. (4) and (5) into Eq. (3) and nondimensionalization, the governing equations become

$$x'' + (1+\mu)f\gamma_1x' - (1+\mu)f^2x + (1+\mu)f^2\beta x^3 - \gamma_2y' - y + (1+\mu)\varepsilon\theta c = 0 \tag{6}$$

$$y'' + \gamma_2y' + y - \mu f\gamma_1x' + \mu f^2x - \mu f^2\beta x^3 - \mu\varepsilon\theta c = p\cos\omega t \tag{7}$$

$$c' + \rho c = \theta x' \tag{8}$$

where the parameters are defined as

$$\omega_1^2 = k_1/m_1; \quad \omega_2^2 = k_2/m_2; \quad \mu = m_1/m_2;$$
$$f = \omega_1/\omega_2; \quad p = Z_0/\omega_2^2\gamma_1; \quad \gamma_1 = d_1/m_1\omega_1$$
$$\gamma_2 = d_2/m_2\omega_2; \quad \theta = \Gamma/L_e; \quad \rho = R_e/L_e\omega_2;$$
$$\varepsilon = L_e/m_1\omega_2^2; \quad \omega = \Omega/\omega_2; \quad \beta = k_3/k_1; \quad t = \omega_2\tau$$

and the operator $()'$ represents a derivative with respect to nondimensional time t.

2.2 Solution Formulation by Harmonic Balance. The method of harmonic balance is applied to solve the governing Eqs. (6)–(8) [27]. To capture the most fundamental dynamics, relative responses of the bistable and linear oscillators and current flow in the circuit can be approximated as

$$x(t) = c_1(t) + a_1(t)\sin(\omega t) + b_1(t)\cos(\omega t) \tag{9}$$

$$y(t) = a_2(t)\sin(\omega t) + b_2(t)\cos(\omega t) \tag{10}$$

$$c(t) = a_3(t)\sin(\omega t) + b_3(t)\cos(\omega t) \tag{11}$$

with slowly varying coefficients. Substituting Eqs. (9)–(11) and their derivatives into (6)–(8), eliminating higher order terms, and grouping the constant, $\sin(\omega t)$ and $\cos(\omega t)$ terms yield seven equations for the coefficient s,

$$-\gamma_1c_1' = f\Lambda_c c_1 \tag{12}$$

$$-\gamma_2a_2' + 2\omega b_2' + \mu f\gamma_1a_1' = -\mu\varepsilon\theta a_3 + \left(1-\omega^2\right)a_2 - \gamma_2\omega b_2 - \mu f^2\Lambda a_1 + \mu f\gamma_1\omega b_1 \tag{13}$$

$$-2\omega a_2' - \gamma_2b_2' + \mu f\gamma_1b_1' = -\mu\varepsilon\theta b_3 + \gamma_2\omega a_2 + \left(1-\omega^2\right)b_2 - \mu f\gamma\omega a_1 - \mu f^2\Lambda b_1 - p \tag{14}$$

$$\gamma_2a_2' - (1+\mu)f\gamma_1a_1' + 2\omega b_1' = (1+\mu)\varepsilon\theta a_3 - a_2 + \gamma_2\omega b_2 + \sum a_1 - (1+\mu)f\gamma_1\omega b_1 \tag{15}$$

$$\gamma_2b_2' - 2\omega a_1' - (1+\mu)f\gamma_1b_1' = (1+\mu)\varepsilon\theta b_3 - \gamma_2\omega a_2 - b_2 + (1+\mu)f\gamma_1\omega a_1 + \sum \mathrm{b}_1 \tag{16}$$

$$-a_3' + \theta a_1' = \rho a_3 - \omega b_3 + \theta\omega b_1 \tag{17}$$

$$-b_3' + \theta b_1' = \omega a_3 + \rho b_3 - \theta\omega a_1 \tag{18}$$

where the terms are defined as

$$\Lambda_c = -1 + \beta\left(c_1^2 + \frac{3}{2}r_1^2\right); \quad \Lambda = -1 + \beta\left(3c_1^2 + \frac{3}{4}r_1^2\right);$$
$$\sum = (1+\mu)f^2\Lambda - \omega^2; \quad r_1^2 = a_1^2 + b_1^2$$

The steady-state response of the system is determined by solving Eqs. (12)–(18). From Eqs. (17) and (18), a_3 and b_3 can be expressed in terms of a_1 and b_1,

$$a_3 = \Phi(\omega a_1 - \rho b_1) \tag{19}$$

$$b_3 = \Phi(\omega a_1 + \rho b_1) \tag{20}$$

where $\Phi = \theta\omega/(\rho^2 + \omega^2)$. Substituting Eqs. (19) and (20) into (15) and (16), a_2 and b_2 can be determined in terms of a_1 and b_1

$$a_2 = \frac{1}{\Delta}[\Gamma_1 a_1 + \Gamma_2 b_1 + (\gamma_2\omega)p] \tag{21}$$

$$b_2 = \frac{1}{\Delta}\left[-\Gamma_2 a_1 + \Gamma_1 b_1 + \left(1-\omega^2\right)p\right] \tag{22}$$

where the terms are defined as

$$\Delta = \left(1-\omega^2\right)^2 + (\gamma_2\omega)^2$$

$$\Gamma_1 = \mu\left[\left(1-\omega^2\right)\left(f^2\Lambda + \varepsilon\theta\omega\Phi\right) + (\gamma_2\omega)(f\gamma_1\omega + \varepsilon\theta\rho\Phi)\right]$$

$$\Gamma_2 = \mu\left[(\gamma_2\omega)\left(f^2\Lambda + \varepsilon\theta\omega\Phi\right) - \left(1-\omega^2\right)(f\gamma_1\omega + \varepsilon\theta\rho\Phi)\right]$$

Substituting Eqs. (19)–(22) into (13) and (14), squaring and summing the resulted equations yield a characteristic equation for r_1^2

$$p^2\left[1 + (\gamma_2\omega)^2\right] = \kappa r_1^2 \tag{23}$$

where κ is defined as

$$\begin{aligned}\kappa = &\left[\left(1-(1+\mu)\omega^2\right)^2 + (\gamma_2\omega)^2\right]\left(f^2\Lambda + \varepsilon\theta\omega\Phi\right)^2 \\ &- 2\omega^2\left[\left(1-\omega^2\right)\left(1-(1+\mu)\omega^2\right) + (\gamma_2\omega)^2\right]\left(f^2\Lambda + \varepsilon\theta\omega\Phi\right) \\ &+ \left[\left\{\left(1-(1+\mu)\omega^2\right)^2 + (\gamma_2\omega)^2\right\}(f\gamma_1\omega + \varepsilon\theta\rho\Phi)^2\right. \\ &\left. + 2\mu\gamma_2\omega^5(f\gamma_1\omega + \varepsilon\theta\rho\Phi) + \omega^4(\gamma_2\omega)^2 + \omega^4\left(1-\omega^2\right)^2\right]\end{aligned}$$

Eq. (23) contains two unknowns c_1 and r_1^2. The constant term may be obtained by solving the steady-state response of Eq. (12). If the bistable device undergoes interwell or high-energy oscillation, the corresponding c_1 is zero. If the response is intrawell oscillation, oscillation around one of its stable equilibria, c_1^2 is found to be

$$c_1^2 = \frac{1}{\beta} - \frac{3}{2}r_1^2 \tag{24}$$

Depending on the dynamics one is interested in, a unique c_1 is substituted into Λ such that Eq. (23) is a function only of r_1^2. The roots of Eq. (23) can then be determined. Solutions are considered to be physically meaningful if the roots are positive, real numbers. Coefficients a_1 and b_1 are explicitly computed after obtaining r_1^2

$$\begin{aligned}a_1 = &\frac{p}{\kappa}\left\{(1+\mu)\gamma_2\omega^3\left(f^2\Lambda + \varepsilon\theta\omega\Phi\right) + \left[1-(1+\mu)\omega^2 + (\gamma_2\omega)^2\right]\right. \\ &\left.\times(f\gamma_1\omega + \varepsilon\theta\rho\Phi) - \gamma_2\omega^5\right\}\end{aligned} \tag{25}$$

$$\begin{aligned}b_1 = &\frac{p}{\kappa}\left\{\left[1-(1+\mu)\omega^2 + (\gamma_2\omega)^2\right]\left(f^2\Lambda + \varepsilon\theta\omega\Phi\right)\right. \\ &\left.- (1+\mu)\gamma_2\omega^3(f\gamma_1\omega + \varepsilon\theta\rho\Phi) - \left(1-\omega^2 + (\gamma_2\omega)^2\right)\omega^2\right\}\end{aligned} \tag{26}$$

The average power density generated by the bistable harvester is then computed as

$$P_1 = \frac{1}{1+\mu}\left[\frac{1}{2}\rho\left(a_3^2 + b_3^2\right)\right] = \frac{\rho}{2(1+\mu)}\frac{\theta^2\omega^2}{(\omega^2+\rho^2)}r_1^2 \tag{27}$$

In the following Secs. 3.1 and 3.2 we employ dimensionless parameters $\rho = 2500$, $\theta = 10$, and $\varepsilon = 0.6$ representative of an electromagnetic generator design having small inductance and moderate transducer coupling constant [23].

To take phase relationships into consideration, steady-state response of Eq. (9) can be alternatively expressed as

$$x = c_1 + r_1\cos(\omega t - \varphi_1); \quad \tan(\varphi_1) = a_1/b_1 \tag{28}$$

2.3 Stability Analysis. To determine the stability of physically meaningful solutions, Eqs. (12)–(18) are cast into the form $\boldsymbol{A}\boldsymbol{x}' = \boldsymbol{F}(\boldsymbol{x})$, where vector $\boldsymbol{x}$ is defined by $\boldsymbol{x} = [a_1, b_1, c_1, a_2, b_2, a_3, b_3]^T$. Stability of response solutions may then be determined by assessing the eigenvalues of the Jacobian of $\boldsymbol{G} = \boldsymbol{A}^{-1}\boldsymbol{F}(\boldsymbol{x})|_{x=x_{ss}}$ [28].

3 Analytical Investigation of Coupling Influences

3.1 Effect of Bistable Harvester Mass Ratio. In this section we investigate how the dynamics and energy harvesting performance of the system are influenced by the ratio of bistable harvester to linear oscillator masses: $\mu = m_1/m_2$. The responses are determined using the system characteristics $p = 0.2$, $f = 0.2$, $\beta = 1$, and $\gamma_1 = \gamma_2 = 0.001$. Previous studies have found that the "magnifier" mass of coupled 2DOF linear harvester systems may be required to be on the order of or greater than that of harvesting element [11–13]; the researchers show that the consequence of the coupled system is not simply amplification of the resonant dynamics but the introduction of new dynamics from which to harvest. Taking the prior insight into account, we consider a large range of mass ratios $\mu = [0.5, 1, 5]$ that reflect the design principles of the earlier work ($\mu < 1$) as well as an alternative design approach ($\mu > 1$) that represents a smaller linear magnifier mass added into the harvesting system. Because steady-state energy harvesting with bistable devices is best accomplished via high-energy dynamics [24], we only consider responses corresponding to interwell vibration. For comparison to the benchmark of the single bistable harvester, we compute the individual bistable device response from its governing equation nondimensionalized using the time of the coupled system $t = \omega_2\tau$

$$x'' + f\gamma_1 x' - f^2 x + f^2\beta x^3 + \varepsilon\theta c = p\cos(\omega t) \tag{29}$$

The corresponding electrical response equation for the single bistable harvester is the same as Eq. (8). Power density is determined from

$$P_1 = \frac{\rho}{2\mu}\frac{\theta^2\omega^2}{(\omega^2+\rho^2)}r_1^2$$

Since our focus is on the energy harvesting potential of the bistable element of the coupled system, for conciseness we omit the corresponding linear oscillator responses. In this and Sec. 3.2 numerically computed results are provided for several of the parameter cases studied. The values are obtained by long-time numerical integrations of the governing Eqs. (6)–(8) and (29) using randomly generated initial conditions. The response amplitudes of the bistable harvester are then computed from the fast Fourier transform of the last 5% of the simulations. The results of 20 simulations yielding single periodic interwell responses are averaged for each data point in Figs. 2 and 3. When more than one form of single periodic interwell response exists at a given excitation frequency, the averaging separates such values for individual determination of amplitudes.

Figure 2 shows the response amplitude and phase between the bistable harvester and linear oscillator and the average power density generated by the bistable harvester component. The response of the individual bistable harvester, without the linear oscillator, relative to base is provided for comparison. Since mass ratio μ is

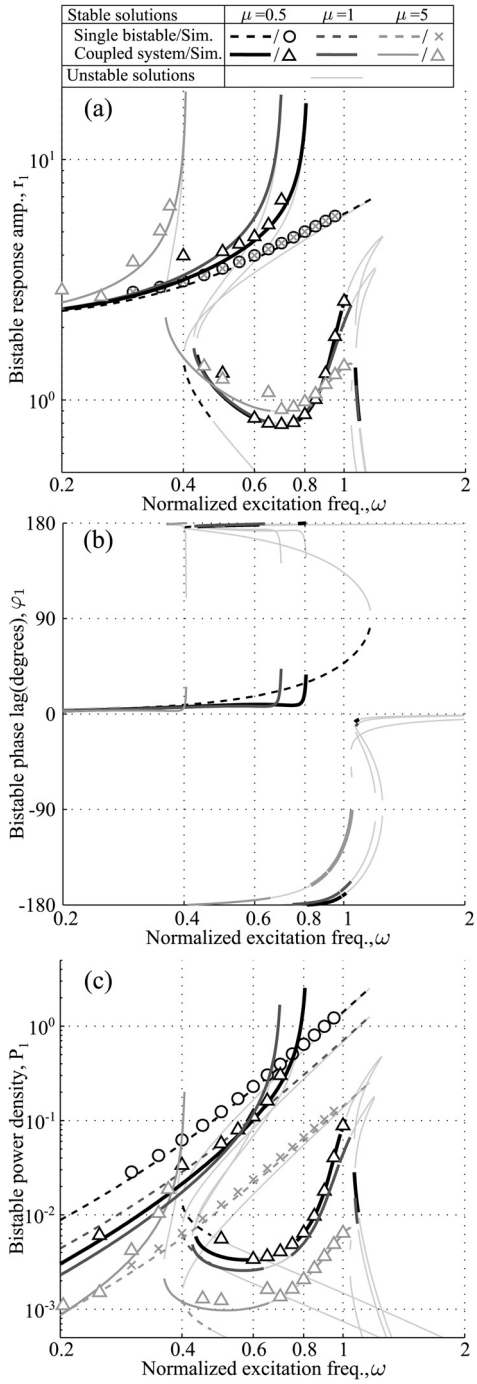

Fig. 2 High-energy dynamics as mass ratio μ varies. Bistable harvester (*a*) displacement amplitude (r_1); (*b*) phase lag (φ_1); and (*c*) average power density (P_1).

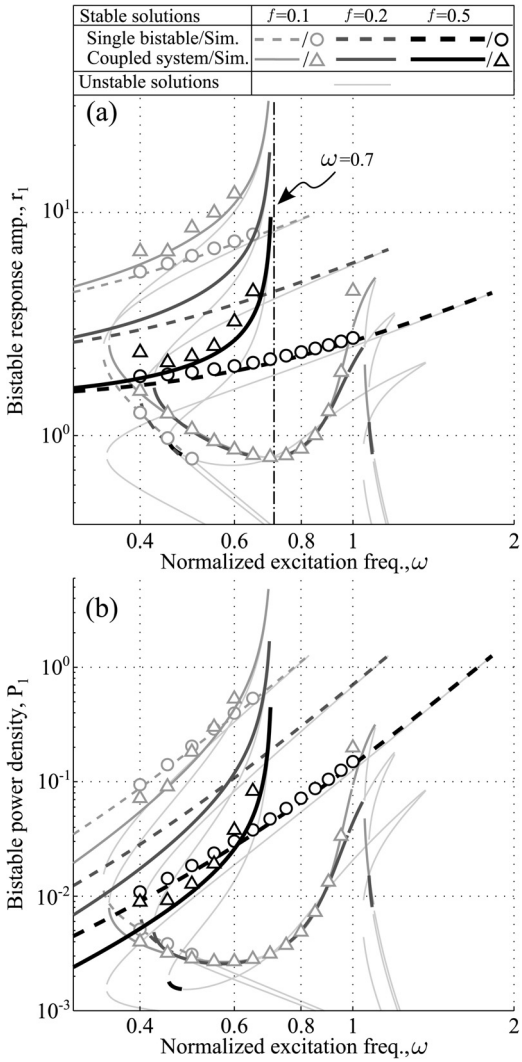

Fig. 3 High-energy dynamics as tuning ratio *f* varies. Bistable harvester (*a*) displacement amplitude (r_1); and (*b*) average power density (P_1).

not presented in Eq. (29), change in μ will not affect the response amplitude of the single bistable harvester. Figure 2(*a*) shows that the coupled system increases the response of the bistable harvester above the baseline of the single bistable device in a frequency band below $\omega^* = 1/\sqrt{1+\mu}$ (see Sec. 4 for more detailed discussion). As the mass ratio μ increases from 0.5 to 5, the amplification of the bistable response for the coupled system becomes more substantial with the trade-off that high-energy dynamics destabilize at lower frequencies. Numerical results are in good agreement with this finding. The reason for destabilization is indicated by the phase relationship. Figure 2(*b*) shows that as driving frequency nears the point at which high-energy dynamics are destabilized, the bistable harvester approaches a 90° phase lag relative to the linear oscillator. Thus the system approaches an in-phase resonance, similar to the lowest mode of a classical linear 2DOF system. We may interpret the influence of the linear oscillator as a variable gain excitation source acting upon the bistable harvester that is dependent on the tuning and mass ratios. Recent work has shown that a bistable harvester cannot sustain large-displacement high-energy dynamics if its response lags the excitation source by more than 90 deg [29]. Since the bistable device high-energy dynamics approach this critical phase lag for the in-phase responses as observed in Fig. 2(*b*), this explains the cause of destabilization of the high-energy response. We also find in Fig. 2(*a*) that the relative amplitude of the bistable device for stable in-phase response remains greater than 1 (greater than the amplitude between the two stable equilibria, determined to be $1/\sqrt{\beta}$ using the definitions from Sec. 2), indicating a snap-through action as opposed to simply moving in-phase with the same response magnitude of the linear resonator. Similar to response amplitude, Fig. 2(*c*) demonstrates that as mass ratio μ increases, the amplification of the power density for coupled system compared with the baseline of the single bistable device becomes more prominent. This trend is *opposite* of that observed for 2DOF linear dynamic magnifier energy harvesting studies [11–13] where it was found that larger added linear DOF (here, $\mu < 1$) serve the greatest benefit to harvesting performance. On the other hand, even for small mass ratio, there still exists a frequency bandwidth where the

coupled bistable harvester average power density exceeds that achieved by the single bistable device.

As the excitation frequency approaches the linear oscillator natural frequency ($\omega = 1$, another branch of stable high-energy dynamics is predicted for the coupled systems, only now they represent out-of-phase response. Increasing mass ratio μ reduces the out-of-phase snap-through response but broadens the stable frequency range. Even though the bistable harvester has exceeded the critical 90 deg phase lag, its snap-through response is characterized by much smaller amplitude unlike the prior high-energy dynamics observed and therefore appears to be a unique phenomenon. We find that in some cases, the bistable harvester response magnitude may be close to the amplitude between the stable and unstable equilibria $r_1 = 1$, for example Fig. 2(*a*) lower amplitude stable branches around $\omega = 0.8$. Since the bistable oscillator exhibits such small snap-through vibrations, this represents a stabilization of the unstable equilibrium position [30–32]. Past study of an appendage linear oscillator for bistable energy harvesting enhancement [26] did not uncover similar advantageous out-of-phase energy harvesting dynamics. This justifies the holistic design perspective as investigations below further support. Lastly, the overall good agreement between numerical and analytical results justifies the effectiveness of utilizing a single term harmonic expansion to capture the essential dynamics of the coupled linear-bistable energy harvesting system.

3.2 Effect of Bistable Harvester Tuning Ratio. To explore the influence of tuning ratio f, we retain parameters of the prior investigations but now consider $\mu = 1$ and $f = [0.1, 0.2, 0.5]$. Figure 3 presents the high-energy dynamics of the bistable harvester with the responses of the corresponding individual bistable device for comparison.

Figures 3(*a*) and 3(*b*) show that two distinct regions of stable high-energy dynamics can be identified: amplified bistable harvester dynamics in a frequency region less than $\omega^* = 1/\sqrt{1+\mu}$ and out-of-phase response around $\omega = 1$ (see Sec. 4 for more detailed discussion). Regardless of the tuning ratio, the amplification effect induced by coupling is observed to be most prominent for frequencies approximately around $\omega \leq 0.7$ with system response destabilized at the same frequency. Simulated results also confirm the trends of amplified response and destabilized interwell dynamics at approximately the same frequency. These findings suggest that the frequency at which in-phase high-energy dynamics of the coupled system are destabilized is primarily controlled by the mass ratio while the tuning ratio principally determines the response amplitude and the rate at which the response asymptotically grows prior to destabilization. The bandwidth of enhanced average power density for the coupled system is likewise unaffected by change in tuning ratio.

As shown in Fig. 3(*a*), tuning ratio is also an important parameter controlling the existence of out-of-phase dynamics for the coupled system around $\omega = 1$. The relative response amplitude between the bistable and linear oscillators of the out-of-phase dynamic is found to decrease as tuning ratio f increases, to the extent that stable response is eventually not possible should tuning ratio become too large. For example, Fig. 3(*c*) predicts that power density generated by the out-of-phase dynamic near $\omega = 1$ is greatest for a tuning ratio of $f = 0.1$, less substantial for $f = 0.2$, but is not possible for $f = 0.5$ since the dynamic is no longer stable. The simulated results likewise corroborate the analytical findings on the influence of tuning ratio in tailoring the existence of out-of-phase response for the coupled system near $\omega = 1$.

3.3 Effect of Bistable Harvester Electromechanical Coupling and System Damping. The influence of electromechanical coupling θ is investigated using system parameters $p = 0.2$, $f = 0.2$, $\beta = 1$, $\mu = 1$, $\gamma_2 = 0.001$, $\gamma_1 = 0.001$, $\rho = 2500$, and $\varepsilon = 0.6$. The coupling is varied over the range $\theta = [5, 10, 20]$ and represent inductive generator designs having

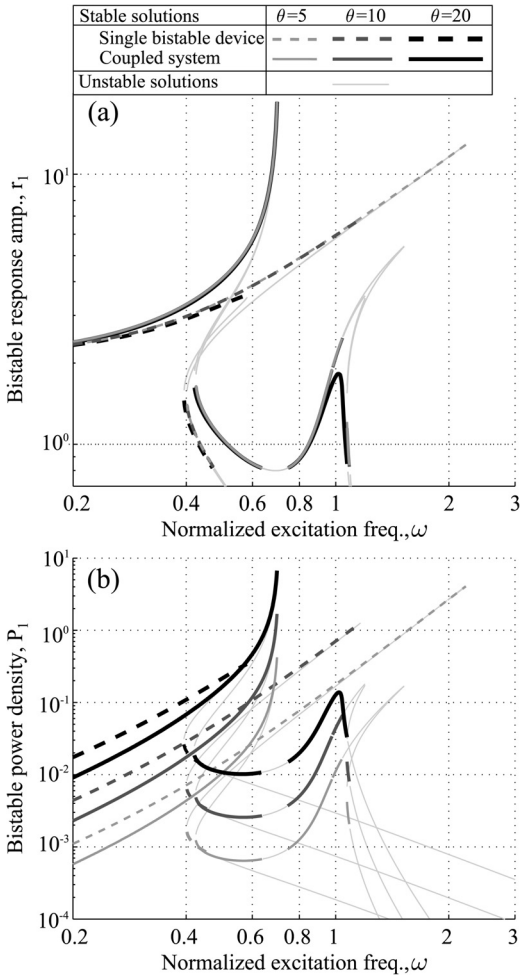

Fig. 4 High-energy dynamics as electromechanical coupling θ varies. Bistable harvester (*a*) displacement amplitude (r_1); and (*b*) average power density (P_1).

moderate to high transducer constants [33], more readily realized for macroscale systems. Figure 4 shows that a drastic degradation on the stable bandwidth of high-energy orbit for the individual bistable harvester is observed as electromechanical coupling θ increases, which is more evident in Fig. 4(*b*). For example, analysis predicts the high-energy orbit of an individual device is sustainable up to approximately $\omega = 2$ with coupling $\theta = 5$ but only possible for $\omega < 0.6$ with $\theta = 20$. This result exemplifies the robustness of the coupled linear-bistable harvester system: for designs utilizing higher electromechanical coupling strengths, the frequency range of high-energy orbit for the coupled system may be greater than that of the single device. The fact that in-phase response of the coupled system destabilizes at the same frequency and grows asymptotically at a similar rate prior to destabilization suggests electromechanical coupling θ is not as important in modifying in-phase dynamics of the bistable harvester as compared to the influence of mass ratio μ and tuning ratio f. Another observation should be made that greater coupling strength θ also plays a role in stabilizing the out-of-phase dynamics. For example, Fig. 4(*a*) predicts that the response remains stable for $\theta = 20$ throughout the entire range of frequencies around $\omega = 1$.

In light of experimental findings in Sec. 5, we lastly consider the consequences of both higher electromechanical coupling $\theta = 20$ and increased mechanical damping in the linear oscillator γ_2 for the high-energy dynamics of the coupled system. We vary γ_2 from 0.001 to 0.1. The in-phase high-energy orbit of the bistable harvester destabilizes at lower frequency as damping of the linear oscillator γ_2 increases, Fig. 5. As a result, the magnitudes of

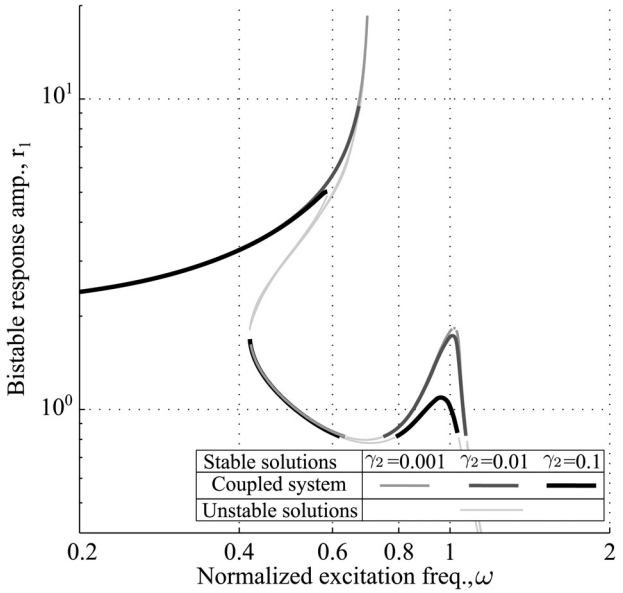

Fig. 5 High-energy dynamics of the bistable harvester in the coupled system as damping in the linear oscillator γ_2 varies

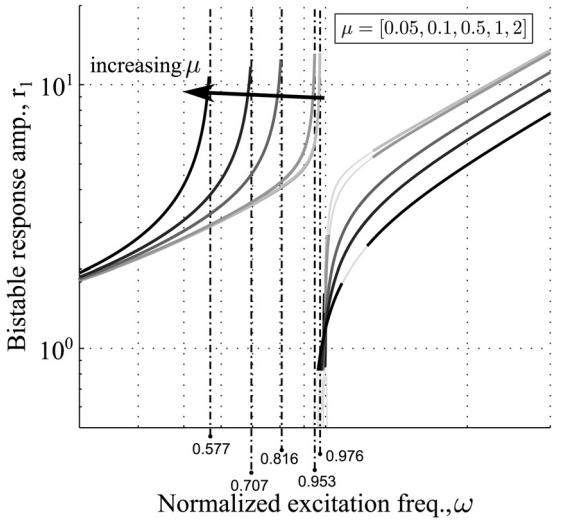

Fig. 6 High-energy dynamics of the bistable harvester in the undamped coupled system as mass ratio μ changes. Bold curves: stable solutions. Thin lines: unstable solutions. Dashed lines represent the predicted frequency of the in-phase snap-through resonance feature.

in- and out-of-phase responses become much closer in amplitude. Overall, this and the prior findings suggest that the magnitude of in-phase high-energy dynamics is governed by the damping influences of the linear oscillator while the amplitude of the out-of-phase high-energy dynamics is primarily influenced by damping effects of the bistable harvester, which may represent either mechanical or electromechanical dissipations.

4 Interpretation of the Induced Frequency Response

The analytical investigations show that the coupled linear oscillator-bistable harvester system yields unique frequency response characteristics. However, like a linear 2DOF system, two resonancelike phenomena are observed when the system has bistability corresponding to the in- and out-of-phase snap-through features apparent in Sec. 3. Figure 2 gives evidence that the mass ratio μ plays a role in determining the frequency at which the first resonance feature appears and that the second resonance effect seems to be fixed around the natural frequency of the uncoupled linear system. Here we confirm this observation, develop guidelines for designing the frequency response characteristics of the coupled linear-bistable harvester system, and provide a new interpretation of the snap-through phenomena.

Bistable snap through may be characterized as a nonresonant phenomenon because any form or frequency of excitation may induce a switching of the mass from one stable state to the other. For a linear 2DOF system, a nonresonant oscillator of finite mass coupled to an excited subsystem may be realized in one of two ways: when the natural frequency of the nonresonant body approaches zero or infinity, $f \to 0$ or $f \to \infty$. For the prior case, the nonresonant oscillator has an infinitesimally small natural frequency, while in the latter case it is infinitely stiff such that it appears to be "welded" to the excited subsystem. Therefore, we may interpret the manner in which the bistable device interacts with the linear oscillator during snap through as being analogous to a linear device of $f \to 0$ and $f \to \infty$.

These perspectives are supported by considering the limiting cases of the undamped linear 2DOF system frequency response [34] as compared to the present results. The characteristic equation governing the resonances of the linear 2DOF system is

$$\omega^4 - \left(1 + f^2(1+\mu)\right)\omega^2 + f^2 = 0 \tag{30}$$

where f and μ are defined as the frequency and mass ratios, respectively, with respect to the excited linear subsystem. Using Eq. (30), a linear body of $f \to 0$ splits the original system resonance into two normalized frequencies $\omega^* = 0$ and 1. Thus, the out-of-phase snap-through response can be interpreted as the response of a linear oscillator with zero natural frequency coupled to an excited linear oscillator since it does not shift the resonant frequency from the uncoupled resonance of the linear system, as observed in Sec. 3. Likewise, for the limiting case $f \to \infty$, only terms multiplied by f^2 in Eq. (30) are appreciable. In this event there are no longer two resonant features but one resonance associated with the composite mass at frequency $\omega^* = 1/\sqrt{1+\mu}$. Hence, in-phase snap-through dynamics of the coupled system may be interpreted as the response of a linear oscillator with infinite natural frequency coupled to the excited linear oscillator since the resonance phenomenon occurs at a frequency associated with the net mass of the system. This defines the frequencies at which the two resonant features of the undamped coupled linear-bistable harvester system occur: one resonant peak at the uncoupled linear natural frequency $\omega^* = 1$ associated with out-of-phase snap through and a second due to the summation of the masses of the linear and bistable oscillators, $\omega^* = 1/\sqrt{1+\mu}$ associated with in-phase snap through.

We validate this perspective by computing the undamped, purely mechanical system dynamics using the model of Sec. 2 with $p = 0.01$, $f = 0.25$, $\beta = 1$. Figure 6 shows the bistable harvester response over a range of mass ratios μ. The frequencies at which the lower resonance characteristics occur are identical to those determined from the expression $\omega^* = 1/\sqrt{1+\mu}$, also confirming earlier observation in Sec. 3.1 that mass ratio predominantly governs where this resonance feature appears; deviation from this exact frequency is therefore a consequence of system damping influences. This shows that snap-through phenomena may be tailored for energy harvesting advantage in the coupled linear-bistable system by adjustment of the mass ratio μ to locate the in-phase high-energy dynamics which amplify the generated power above that achievable by the single bistable harvester. The resonance feature associated with out-of-phase snap through, which occurs at the uncoupled natural frequency of the linear oscillator $\omega = 1$, is attained without specific design requirements, as had been observed in Sec. 3.3 even in the presence of high damping in both components of the system. Since the previously studied energy harvester configuration employed a directly

excited bistable harvester with add-on linear oscillator [26], and given that a directly excited bistable system may lag its excitation source by no greater than 90 deg to sustain large-displacement high-energy dynamics, the previously studied harvester configuration [26] cannot obtain the advantageous out-of-phase high-energy response of the present system. This exemplifies the performance enhancement and versatility of the present coupled linear-bistable harvester system approach.

5 Experimental Investigation

The results of Sec. 3 indicated the coupled linear oscillator-bistable harvester system could (i) amplify low excitation levels to intensify in-phase snap through and also (ii) yield an out-of-phase snap through response around the linear oscillator uncoupled natural frequency. These two results can enhance energy harvesting performance and are shown to be tailored for fixed excitation level by adjusting mass ratio μ, electromechanical coupling θ, and tuning ratio f. Here we validate these key analytical trends by experiments.

A photograph of the test setup is shown in Fig. 7. The linear oscillator mass is composed of the machined aluminum frame, bottom bearing mass, and bistable oscillator bearing guide rail. The bistable mass is composed of the bearing mass in the middle of the photograph along with the hardware necessary to affix the mass to the attached spring. The bistable oscillator is developed by precompressing the spring (in its upright position) between the bistable inertial mass and a rotational pivot affixed to the linear oscillator. Therefore, the two stable equilibria for the bistable mass are to the right and left of the central unstable position. Guide rods are used to prevent the precompressed spring from bending or twisting as the inertial mass snaps from one stable state to the other. Both linear and bistable oscillators utilize low-friction linear slide bearings. An adjustable, translational pneumatic damper is used to modify the damping between the linear oscillator and bistable harvester. The coupled system is mounted to an electrodynamic shaker table activated in the horizontal left–right direction. The linear oscillator natural frequency is approximately 6 Hz. The shaker excitation during tests is a slowly forward swept sinusoid from 1 to 9 Hz (+0.025 Hz/s). To compare the dynamics of a single bistable oscillator to the same input conditions, the linear oscillator is locked to the shaker platform by preventing motion of the bottom linear bearing. Three accelerometers measure the dynamics of the shaker platform and linear and bistable oscillators.

5.1 Effect of Bistable Harvester Electromechanical Coupling. For inductive vibration generators when the inductance is small (i.e., the electrical natural frequency is substantially greater than the mechanical natural frequency) which is common for many macroscale electromagnetic harvesters, the governing equations may be reduced by direct substitution of the electrical response Eq. (8) into Eqs. (6) and (7) by the relation $c = (\theta/\rho)x'$ [35]. Defining a coupling factor $\kappa_c = \theta/\rho$ the effect of electromechanical responses on bistable harvester dynamics is then modeled as additional damping, where the total damping is $\gamma = \gamma_1 + \kappa_c^2$. Consequently, in the following experiments, we investigate the influence of changing electromechanical coupling by adjustment of total damping γ between the linear oscillator and bistable harvester.

Figure 8 plots the measured acceleration frequency response functions (frf) as the bistable damping γ varies. For the single bistable oscillator, this is the ratio of relative accelerations between the bistable inertial mass and shaker table to the shaker input acceleration; for the coupled system, this is the ratio of the relative acceleration between the bistable and linear elements to the shaker acceleration. Only high-energy dynamics are plotted. The sweep test is conducted with input rms acceleration of 2.83 m/s^2. As depicted in Fig. 8, the high-energy response of the single bistable device destabilizes at progressively lower frequencies as damping increases. In contrast, the in-phase dynamics of the coupled system are much less sensitive to increase in the damping, in agreement with analytical trend predicted in Fig. 4.

While the single bistable system exhibits only low-energy dynamics for excitation frequencies greater than the maximum sustainable interwell oscillation frequency (4 to 5 Hz), the coupled systems undergo another energetic out-of-phase high-energy dynamic around the natural frequency of the linear oscillator. As bistable damping increases, the peak vibrational amplitude of this dynamic decreases, confirming model predictions in Sec. 3.3. Lastly, Fig. 8 shows that the magnitudes of in- and out-of-phase high-energy dynamics of the bistable oscillator are on the same order of magnitude. As was explored in Sec. 3.3, this indicates that the levels of damping are relatively high in both the linear and bistable oscillator bearings.

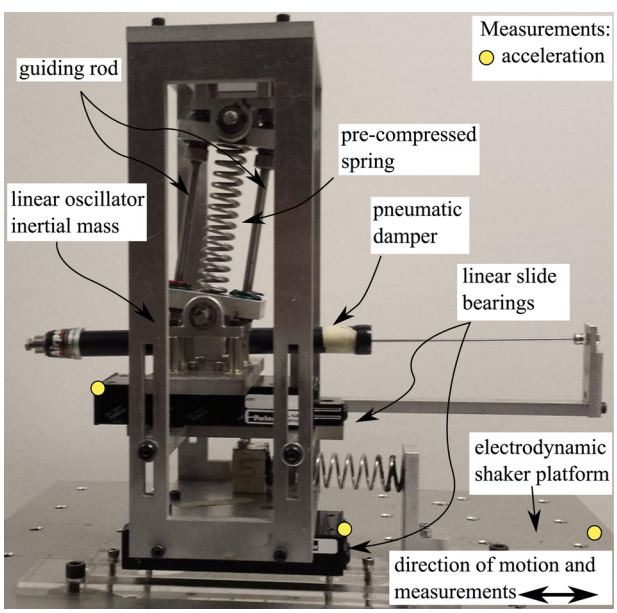

Fig. 7 Photograph of linear-bistable coupled system showing elements of system configuration and test setup

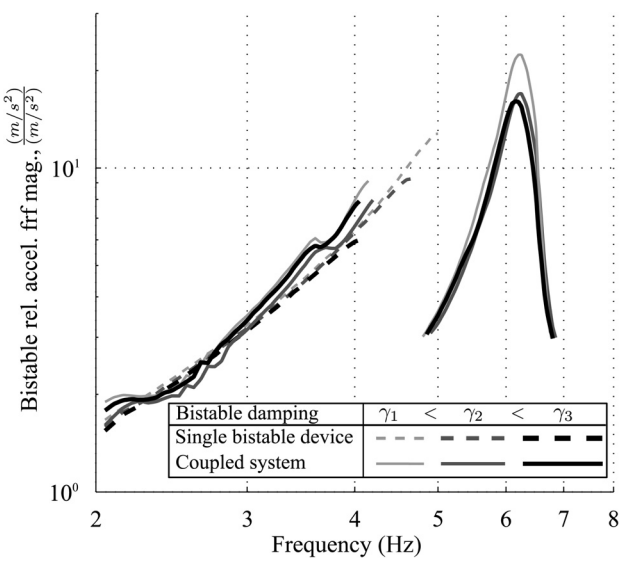

Fig. 8 Relative acceleration frf of the bistable oscillator inertial mass as a function of damping between linear oscillator and bistable harvester

5.2 Effect of Bistable Harvester Mass. As observed in Secs. 3 and 4, mass ratio μ is important in terms of determining the frequency at which in-phase snap through destabilizes. In this investigation we validate the trend by changing bistable mass. However, direct change in mass in experiments additionally influences the bistable linear natural frequency and thus changes other nondimensional parameters such as f, γ_1, and ε. To facilitate comparing trends between analysis and experiment, we first plot in Fig. 9(*a*) the analytically predicted response amplitude of the bistable harvester as bistable mass varies. The bistable harvester vibration amplitude for the coupled system is always enhanced as compared to the single bistable harvester. As the bistable mass increases, in-phase interwell dynamics destabilize at lower frequency for both the coupled and single bistable systems. In contrast, out-of-phase dynamics for the coupled system are less sensitive to change in bistable mass as compared with change in mass ratio μ as found in Fig. 2(*a*).

Having an understanding of the specific influence of bistable mass as predicted by analysis, Fig. 9(*b*) plots the measured acceleration frequency response functions (frf) as bistable mass varies with input rms acceleration of 2.07 m/s^2. Each of the prior analytical trends can be verified from the data. First, a frequency range may consistently be found where response amplitude for the coupled system is amplified above that of the single bistable device. Next, the in-phase response for both coupled and single bistable systems destabilize at progressively lower frequency as the bistable mass increase. Lastly, the out-of-phase response for the coupled system is insensitive to the change of bistable mass. These findings thoroughly support the analyses and help to demonstrate the advantages of the coupled linear-bistable system configuration for more robust energy harvesting performance.

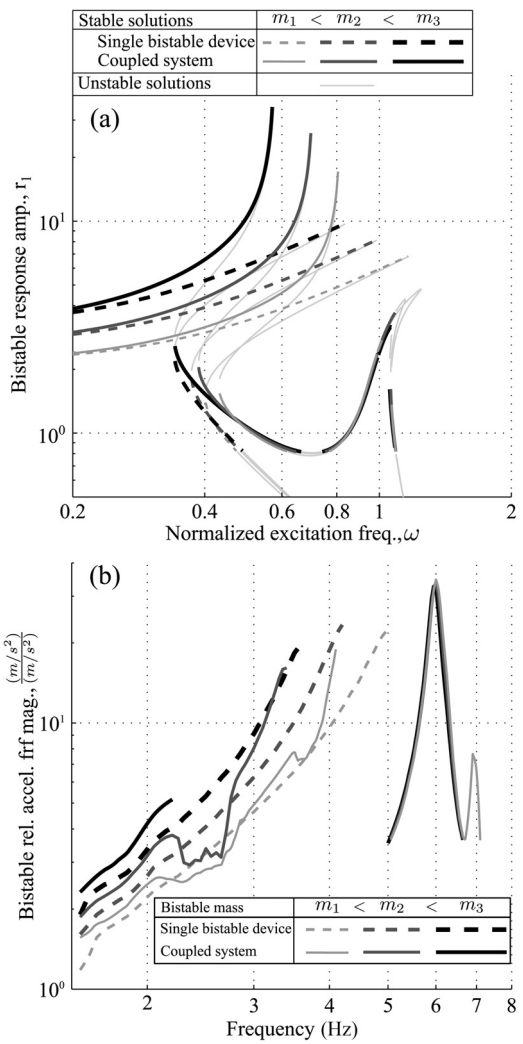

Fig. 9 High-energy dynamics of the bistable harvester in the coupled system as bistable mass varies. (*a*) Bistable harvester displacement amplitude (r_1); and (*b*) relative acceleration frf of the bistable oscillator inertial mass as a function of bistable mass.

6 Conclusion

This paper presented an analytical, numerical, and experimental study of the synthesis of a coupled linear oscillator and bistable energy harvester system. Investigations revealed that with the coupled system, in-phase interwell vibration and power density of the bistable harvester are enhanced dramatically for excitation frequencies in a bandwidth less than the resonant frequency of the linear oscillator having a mass that is the sum of linear and bistable bodies. It was found that mass ratio μ primarily determines the frequency at which the coupled system loses the capability to sustain in-phase high-energy dynamics while tuning ratio f mainly determines the response magnitude and rate at which the amplification grows close to the in-phase snap-through feature. When the excitation frequency is close to the resonance of the uncoupled linear oscillator, a second stable out-of-phase high-energy dynamic may be induced. It is shown that as electromechanical coupling θ increases, the bistable harvester dynamics of the coupled system remain relatively unaffected as compared to the reduced response bandwidth of the individual bistable harvester, providing an opportunity to harvest more energy from the coupled system. Numerical simulations and experiments validated key analytical trends observed throughout analyses. The results of this work justify the holistic design approach in developing linear-bistable coupled systems for enhancing the performance and robustness of bistable energy harvesters.

Acknowledgment

This research is partially supported by the Defense Advanced Research Projects Agency (DARPA) under Contract No. HR0011-10-C-0148, subcontracted via the Teledyne Scientific Company (TSC).

References

[1] Cook-Chennault, K. A., Thambi, N., and Sastry, A. M., 2008, "Powering MEMS Portable Devices—A Review of Non-Regenerative and Regenerative Power Supply Systems With Special Emphasis on Piezoelectric Energy Harvesting Systems," Smart Mater. Struct., **17**(4), p. 043001.
[2] El-Hami, M., Glynne-Jones, P., White, N. M., Hill, M., Beeby, S., James, E., Brown, A. D., and Ross, J. N., 2001, "Design and Fabrication of a New Vibration-Based Electromechanical Power Generator," Sensors Actuators A Phys., **92**(1–3), pp. 335–342.
[3] Roundy, S., Wright, P. K., and Rabaey, J., 2003, "A Study of Low Level Vibrations as a Power Source for Wireless Sensor Nodes," Comput. Commun., **26**(11), pp. 1131–1144.
[4] Mitcheson, P. D., Green, T. C., Yeatman, E. M., and Holmes, A. S., 2004, "Architectures for Vibration-Driven Micropower Generators," J. Microelectromech. Syst., **13**(3), pp. 429–440.
[5] Tang, L., Yang, Y., and Soh, C. K., 2010, "Toward Broadband Vibration-Based Energy Harvesting," J. Intell. Mater. Syst. Struct., **21**(18), pp. 1867–1897.
[6] Zhu, D., Tudor, M. J., and Beeby, S. P., 2010, "Strategies for Increasing the Operating Frequency Range of Vibration Energy Harvesters: A Review," Meas. Sci. Technol., **21**(2), p. 022001.
[7] Zuo, L., 2009, "Effective and Robust Vibration Control Using Series Multiple Tuned-Mass Dampers," ASME J. Vib. Acoust., **131**(3), p. 031003.
[8] Moheimani, S. O. R., 2003, "A Survey of Recent Innovations in Vibration Damping and Control Using Shunted Piezoelectric Transducers," IEEE Trans. Control Syst. Technol., **11**(4), pp. 482–494.
[9] Tang, L., and Yang, Y., 2012, "A Multiple-Degree-of-Freedom Piezoelectric Energy Harvesting Model," J. Intell. Mater. Syst. Struct., **23**(14), pp. 1631–1647.
[10] Abdelkefi, A., Nayfeh, A. H., Hajj, M. R., and Najar, F., 2012, "Energy Harvesting From a Multifrequency Response of a Tuned Bending–Torsion System," Smart Mater. Struct., **21**(7), p. 075029.
[11] Aldraihem, O., and Baz, A., 2011, "Energy Harvester With a Dynamic Magnifier," J. Intell. Mater. Syst. Struct., **22**(6), pp. 521–530.

[12] Aladwani, A., Arafa, M., Aldraihem, O., and Baz A., 2012, "Cantilevered Piezoelectric Energy Harvester With a Dynamic Magnifier," ASME J. Vib. Acoust., **134**(3), p. 031004.
[13] Zhou, W., Penamalli, G. R., and Zuo, L., 2012, "An Efficient Vibration Energy Harvester With a Multi-Mode Dynamic Magnifier," Smart Mater. Struct., **21**(1), p. 015014.
[14] Tang, X., and Zuo, L., 2011, "Enhanced Vibration Energy Harvesting Using Dual-Mass Systems," J. Sound Vib., **330**(21), pp. 5199–5209.
[15] Wu, H., Tang, L., Yang, Y., and Soh, C. K., 2013, "A Novel Two-Degrees-of-Freedom Piezoelectric Energy Harvester," J. Intell. Mater. Syst. Struct., **24**(3), pp. 357–368.
[16] Masana, R., and Daqaq, M. F., 2011, "Relative Performance of a Vibratory Energy Harvester in Mono- and Bi-Stable Potentials," J. Sound Vib., **330**(24), pp. 6036–6052.
[17] Ramlan, R., Brennan, M. J., Mace, B. R., and Kovacic, I., 2009, "Potential Benefits of a Non-Linear Stiffness in an Energy Harvesting Device," Nonlinear Dyn., **59**(4), pp. 545–558.
[18] Erturk, A., Hoffmann, J., and Inman, D. J., 2009, "A Piezomagnetoelastic Structure for Broadband Vibration Energy Harvesting," Appl. Phys. Lett., **94**(25), p. 254102.
[19] Stanton, S. C., McGehee, C. C., and Mann, B. P., 2010, "Nonlinear Dynamics for Broadband Energy Harvesting: Investigation of a Bistable Piezoelectric Inertial Generator," Phys. D, **239**(10), pp. 640–653.
[20] Arrieta, A. F., Hagedorn, P., Erturk, A., and Inman, D. J., 2010, "A Piezoelectric Bistable Plate for Nonlinear Broadband Energy Harvesting," Appl. Phys. Lett., **97**(10), p. 104102.
[21] Gammaitoni, L., Neri, I., and Vocca, H., 2009, "Nonlinear Oscillators for Vibration Energy Harvesting," Appl. Phys. Lett., **94**(16), p. 164102.
[22] Tang, L., Yang, Y., and Soh, C.-K., 2012, "Improving Functionality of Vibration Energy Harvesters Using Magnets," J. Intell. Mater. Syst. Struct., **23**(13), pp. 1433–1449.
[23] Mann, B. P., Barton, D. A., and Owens, B. A., 2012, "Uncertainty in Performance for Linear and Nonlinear Energy Harvesting Strategies," J. Intell. Mater. Syst. Struct., **23**(13), pp. 1451–1460.
[24] Harne, R. L., and Wang, K. W., 2013, "A Review of the Recent Research on Vibration Energy Harvesting Via Bistable Systems," Smart Mater. Struct., **22**(2), p. 023001.
[25] Tang, L., Yang, Y., and Wu, H., 2012, "Modeling and Experiment of a Multiple-DOF Piezoelectric Energy Harvester," SPIE Proceedings, Vol. 8341, Active and Passive Smart Structures and Integrated Systems 2012, Paper No. 83411E.
[26] Harne, R. L., Thota, M., and Wang, K. W., 2013, "Bistable Energy Harvesting Enhancement With an Auxiliary Linear Oscillator," Smart Mater. Struct., **22**(12), p. 125028.
[27] Virgin, L. N., 2000, *Introduction to Experimental Nonlinear Dynamics: A Case Study in Mechanical Vibration*, Cambridge University Press, New York.
[28] Nayfeh, A. H., and Mook, D. T., 1979, *Nonlinear Oscillations*, John Wiley, New York.
[29] Harne, R. L., Thota, M., and Wang, K. W., 2013, "Concise and High-Fidelity Predictive Criteria for Maximizing Performance and Robustness of Bistable Energy Harvesters," Appl. Phys. Lett., **102**(5), p. 053903.
[30] Kim, S.-Y., and Kim, Y., 2000, "Dynamic Stabilization in the Double-Well Duffing Oscillator," Phys. Rev. E, **61**(6), pp. 6517–6520.
[31] Kim, Y., Lee, S. Y., and Kim, S.-Y., 2000, "Experimental Observation of Dynamic Stabilization in a Double-Well Duffing Oscillator," Phys. Lett. A, **275**(4), pp. 254–259.
[32] Wu, Z., Harne, R. L., and Wang, K. W., "Excitation-Induced Stability in a Bistable Duffing Oscillator: Analysis and Experiments," ASME J. Comput. Nonlinear Dyn. (submitted).
[33] Cassidy, I. L., Scruggs, J. T., Behrens, S., and Gavin, H. P., 2011, "Design and Experimental Characterization of an Electromagnetic Transducer for Large-Scale Vibratory Energy Harvesting Applications," J. Intell. Mater. Syst. Struct., **22**(17), pp. 2009–2024.
[34] Den Hartog, J. P., 1985, *Mechanical Vibrations*, Dover, New York.
[35] Daqaq, M. F., 2011, "Transduction of a Bistable Inductive Generator Driven by White and Exponentially Correlated Gaussian Noise," J. Sound Vib., **330**(11), pp. 2554–2564.